# A 1D helical eco-friendly Mn(II) halide coordination polymer: Luminescent properties involving resonant energy transfer and magnetic characterization

Dhouha Abid, Haitham Abid, Wassim Maalej, El kebir Hlil, Philippe Guionneau, Stanislav Pechev, Nathalie Daro, Zakaria Elaoud

# A 1D helical eco-friendly Mn(II) halide Coordination Polymer: luminescent properties involving Resonant Energy Transfer and magnetic characterization

ABID Dhouha [1], ABID Haitham [2], MAALEJ Wassim[1], HLIL Elkebir [3], GUIONNEAU Philippe [4], PECHEV Stanislav [4], DARO Nathalie[4], ELAOUD Zakaria [1*]

[1] Laboratory Physical-Chemistry of Solid state, University of Sfax, Faculty of Sciences of Sfax, Tunisia

[2] Laboratory of Applied Physics University of Sfax, Faculty of Sciences of Sfax, Tunisia

[3] Institut Neel, CNRS - Université J. Fourier, BP. 166, 38042 Grenoble, France

[4] CNRS, Univ. Bordeaux, ICMCB, 87 avenue of Dr A. Schweitzer, 33608 Pessac, Bordeaux, France

**ABSTRACT**

In the present work, we discuss the synthesis of nontoxic Mn(II) halide coordination polymer and explore the potential light emission properties for solar-cell devises through experimental and computational studies. The crystal structure was unveiled through Single Crystal Diffraction, whereas physical properties were investigated by means of thermal, spectroscopic, magnetic, optical and photoluminescence measurements. The observed left-right handed helical structure is built up from an infinite 1-D chains of Mn(II) octahedra. The polymeric network is stabilized through inter-molecular hydrogen bonding interactions and π···π face-to-face interactions. Furthermore, ferro-antiferromagnetic ordering has been proven through magnetic measurements. A deep investigation of the photoluminescence study reveals the presence of a bright bluish light emission with corresponding CIE color coordinates of (0.27, 0.35), CCT value of 8092 K and a very high CRI value of 96. The origin of this intense light emission is mainly attributed to the occurrence of the resonant energy and charge transfer processes between Triazolate ligand and inorganic Mn-Cl sub-lattices. Such behavior leads to the conversion of Frenkel excitons localized within the organic part to Mott-Wannier excitons localized in inorganic clusters. Based on these results, we strongly believe that the elaborated material can be a promising candidate for eco-friendly electronic applications.

**KEYWORDS :** Coordination polymer, left-right helical, photoluminescence, bright light emission, CIE color, resonant energy.

## INTRODUCTION

Solid-State Lighting (SSL) has recently emerged as one of the foremost vital technologies that can greatly improve our daily lives due to its energy-saving, compactness, high efficiency and eco-friendliness. Being made through yellow phosphor coated blue LEDs or red, green and blue phosphor integrated UV LEDs. The currently commercialized SSLs are commonly white light-emitting diodes (LEDs) [1–4]. However, these strategies used to achieve white emission have many drawbacks, such as reduced self-absorption efficiency, changes in emission color, attenuation of individual components, and reduced color rendering. Taking all this into consideration, the development of single-component emitters seems to strongly stimulate the vast-ranged scientific community to further synthesize white luminescent materials with high stability, excellent color rendering and high luminous efficiency [5,6].

In particular, halide-based hybrid materials have gained tremendous attention due to their unusual structural diversity and outstanding optoelectronic properties. These materials have exhibited interesting properties in many technological applications in different fields, including WLEDs, laser cooling, light-emitting transistors, and photovoltaic solar cells [11-16].

Recently, lead halide hybrid perovskite materials have attracted much attention because of their photoluminescent and optoelectronic properties[16-21]. Among them, Elleuch et *al.* and Mitzi et *al.* synthesed perovskite-like materials with the general formula $(TAE)_2[Pb_2Cl_{10}](Cl)_2$[22] and $(H_2AEQT)PbCl_4$ [23], respectively. These latter that showed the highest CRI and important efficient solid state solar cells absorber. Despite their remarkable performance, lead halide hybrid perovskite materials have been limited in their practical applications due to the environmental concerns and pollution about employing toxic metals like Pb(II) [24]. In order to resolve this issue and to reduce environmental pollution, scientific researchers have attempted to find a feasible alternative for lead. In particular, luminescent halide-based coordination polymers are identified as a new and ideal candidate for WLEDs due to their wide range of structural diversity and exotic optical functionalities. Their various self-assembly modes, multiple emitting centers, and their friendly environments, that benefit from the combination of organic ligands and non-toxic metal nodes, makes them a highly emissive candidate[25-31]. Besides, the short coordination links between organic ligands and inorganic entities as well as the nature of the organic linkers will foster the appearance of resonance energy transfer (FRET) which is the main responsible for the WL emission process [33]. At present, only a few WLED hybrid coordination polymers have been investigated so far. W. Ouellette et *al.* have reported a series of 3-D crystalline structures based on copper with

the formula $[Cu_2(Trz)Br_2]$[34] and $[Cu_3(Trz)_4(H_2O)_3]F_2$[34] $[Cu_3(Trz)_3OH][Cu_2Br_4]$ [34] that demonstrate a good photo-physical properties and bright light emission. In 2022, a coordination polymer based on copper with the general formula $\{[(CuI)(Hptdp)]_4 \cdot H_2O\}_n$[31] prepared by Yu, M.X. et *al.* revealed an exceptional helical structure and a dual white light emission process, a CCT of 3632 K and a CRI of 93.4. Regarding these previously reported research, only a limited number of Mn-based Wight light absorbing coordination polymers have been investigated so far.

Aside from these targeted optoelectronic properties, magnetic properties can also be introduced into these crystalline coordination polymers through an adequate selection of the organic ligands and the functional nodes, which makes them potential candidates for various applications including electromagnets, and electromagnetic wave propagation[35-41].

As part of our ongoing research and in order to improve these findings, we report a novel one-dimensional non-toxic Mn(II) hybrid halide coordination polymer with the general formula $Mn(\mu_2\text{-}Trz)(\mu_2\text{-}Cl_2)$, that exhibits impressive bluish light emission properties, and the highest CRI value. The crystal structure, thermal decomposition, spectroscopic analysis, magnetic properties were investigated. Photo-physical studies of the title compound as well as the Trz.Cl organic salt supported by density functional theory calculation were investigated in order to fully understand the origin of the bluish light emission process and explore these results toward the development of light emitting diodes.

## 1. EXPERIMENTAL DETAILS

### 1.1. Synthetic approaches

Chemical reagents were purchased from a commercial source (Sigma-Aldrich) and used as received without further purification: Manganese (II) chloride tetrahydrate ($MnCl_2.4H_2O$, 99%), 1,2,4 Triazole ($C_2H_3N_3$, 98%).

An aqueous solution of $MnCl_2.4H_2O$ (13.8 mg, 0.7 mmol) was added dropwise to an ethanolic solution of Trz (0.34 mg, 0.5 mmol) with stirring. The mixed solution was transferred in a Teflon-lined stainless-steel autoclave, heated at 150 °C for 2 days under autogenous pressure. The resulting white crystals were filtered, washed with distilled water and ethanol five times in order to remove all extra impurities. Finally, crystals were dried at 40°C in a vacuum oven for 15 h. The SEM images of the synthesized crystals are reported in **Figure S1**.

### 1.2. Thin-film preparation

Thin-films of Mn(II)-based complex were prepared through the spin coating technique. Crystals were dissolved in 1.5 ml of ethanol and then spin-coated on solid quartz at 2500 rpm for 10 s. The prepared film was then annealed at 90 °C in order to remove the residual ethanol solvent.

### 1.3. Single Crystal X-ray data collection

A single crystal of Mn($\mu_2$-Trz)($\mu_2$-$Cl_2$) with dimensions (0.3x0.25x0.15) was selected under a polarizing microscope and measured with Bruker Kappa APEX II diffractometer using Mo-Kα radiation (λ= 0.71073 Å). Intensity data were collected at 293 K in the $3.4\ ° \leq \theta \leq 27.5\ °$ range. The crystal structure was solved in the orthorhombic system with the centro-symmetric space group Imma. Metal transition atom Mn(II) was fixed using Patterson method with the SHELXS-97 program[41] within the WINGX crystallographic software[42] Nitrogen, carbon and chloride atoms were found from successive Fourier calculations and refined during the final cycles with anisotropic thermal parameters using the SHELXL-2018 [44] (Sheldrick 2018) program. Aromatic hydrogen atom positions were calculated using a riding model, with N–H = 0.86 Å and C–H = 0.93 Å. Furthermore, the structural graphics were made using the OLEX2 [45] and Diamond programs [46].

Crystallographic details for the Mn(II)-based complex are summarized in **Table S1**. Atomic positional parameters and anisotropic factors ($U_{eq}/U_{iso}$) and full tables of selected bond lengths and angles are depicted in the supporting information file (**Tables S2** and **S3**).

### 1.4. Thermal analyses and IR Spectroscopy

The thermal stability of the coordination polymer was investigated through TGA measured under $O_2$ atmosphere at a heating rate of 10°C $min^{-1}$. Measurements were performed by heating 3.081 mg of a powdered sample from 303K to 773K. The differential scanning calorimetry (DSC) measurements were performed in air atmosphere using a SETARAM differential scanning calorimeter of the STA 449C type.

FT-Infrared measurements were recorded in frequency ranges 400-4000 $cm^{-1}$ using a Perkin-Elmer FT-IR Spectrum at room temperature. The solid compound was pressed into pellets after dilution with KBr.

### 1.5. Magnetic measurements

Magnetic studies were conducted using Quantum Design MPMS3 SQUID magnetometer developed at Louis Néel Laboratory. Measurements were carried out in a temperature range of 2-400 K under a magnetic field of 499.7 Oe. Isothermal M(H) data were conducted at 2K in the field range of 0= ±11 kOe.

### 1.6. Optical measurement

Solid states room temperature photoluminescence measurements (Pl) were recorded using a JOBIN YVON HR 320 spectrophotometer under 266 nm excitation wavelength.

Three main characteristics are used in order to define the white light stability. The first one is the "CIE" (Commission Internationale d'Eclairage) parameter, which is the most frequently used approach for describing the constituents of any color based on the three primaries (green, blue and red) coordinates. The second and third parameters are the ‘’CCT’’ (Correlated Color Temperature), which measures the color appearance of a light source and the “CRI” (the Color Rendering Index) is a numerical value that describes the appearance of the color to the naked eye when irradiated through a light source.

The optical absorption measurements (OA) of the complex and Trz.Cl salt was performed at ambient conditions on spin-coated film using a conventional UV−vis spectrophotometer (HITACHI, U3300).

Room temperature photoluminescence excitation (PLE) was performed on a Fluoromax-4 Spectro-fluorimeter equipped with a xenon lamp as an excitation source.

### 1.7. Computational methods

DFT calculation were conducted using the Wien2k package. The Kohn-Sham equation was solved using all-electron full-potential linearized augmented plane wave. The radius of Muffin-Tin (RMT) was chosen to be 2.2, 1.6, 0.9, 1.1 and 0.53 a.u for Mn, Cl, C, N, respectively. The plane wave cutoff value of Kmax = 3/RMT was taken for a wave function in the interstitial region. Convergence was checked via self-consistency. The convergence was achieved for less than 0.01 mRyd per formula unit.

## 2. RESULTS AND DISCUSSION

### 2.1. Insight into the structure Aspects

The X-ray single crystal diffraction analysis reveals that the coordination polymer crystallizes in the orthorhombic space group Imma and features a novel 1D framework. As shown in **Figure S2**, the form unit is made up of one Mn(II) atom, one fully aromatic Trz ligand, and one guest of chloride anion. The Mn(II) center exhibit $\{MnN_2Cl_4\}$ distorted octahedral geometry. Within this polyhedron, four Cl anions fill the equatorial plan, while the axial sites are occupied by two donor nitrogen atoms arising from chelating Trz group ($N_1$, $N_1$'). As represented in **Table S2**, the axial Mn-N and Mn-Cl bond lengths are 2.229 (7) and 2.5659 (2), respectively. These Mn-N bond distance are very close the Mn-N distance of 2.2403(1)- 2.2473(1) observed in the $H[Mn_6(BTA)_8Cl_5] \cdot (H_2O)_4$ complex [41]. In addition, the Cl-Mn-Cl bite angles range from 87.80 (2)° to 180°, exhibit significant deviation from ideal octahedral bite angles and those of N-Mn-N formed by nitrogen atoms in trans-position are 180°. These facts clearly justify the distortion of the ideal octahedral geometry around Mn (II) centers and assume an axially compressed polyhedron. Such phenomenon is due to the Jahn-Teller effect. Therefore, the calculated mean values of the distortion indices for these two octahedral are $ID_{d(metal\ -\ ligand)}$ = 0.0137 Å. These values are calculated using the following formula : $ID_d = \sum(|\frac{di-dm}{n.dm}|)$, where, di : the Mn-ligand bond length. Bond distances and angles between metal and ligands are comparable to those found in previously reported M(II)-based compounds [47-50]. The $\{MnN_2Cl_4\}$ octahedral are edge-sharing via two chloride atoms to form centrosymmetric dimers. In addition, the value of the cis angle varies from 83.96 (6) to 84.79 (5) °, respectively. Such results are due to the electrostatic repulsion between neighboring metal cations. Thus, the shortest intermetallic distance separating two metallic polyhedra Mn… Mn is of the order of 3.4156 Å (**Figure 1**) which may reflect interesting magnetic interactions.

Generally, The Trz ligand and its derivatives form easily a poly-nuclear cluster through their various bridging modes. They are also known to crystallize by forming 1-D chains [51,52]. In our title complex, the Trz rings adopt a bis-chelating $\mu_2$:$\eta^1$:$\eta^1$ mode bridging the two metallic centers via the $N_1$, $N_1$'-sites. Besides, each chloride ions adopt a $\mu_2$-Cl bridging fashion. Interestingly, these various coordination modes give birth to an infinite double left-right handed helical 1D chain (α, β-helix) stacking along the *b* axis direction (**Figure 2**).

Furthermore, the study of the crystal packing of the material clearly reveals that the polymeric network is stabilized through intermolecular hydrogen bonding interactions. In fact, the aromatic Trz ligands are connected to the chloride ions through two types of hydrogen bonds: N–H…Cl and C–H…Cl. Distances and bond angles characterize the hydrogen bonds are reported in **Table S4.** Moreover, the helical coordination polymers are stabilized through π…π interactions particularly face-to-face interactions along the *b*-axis arising between two adjacent aromatic Trz ligands generatrf from two successive chains. The inter-planar distances between two centroids ($dcg_1…cg_2$) are approximately 3.5976 Å (**Figure S3**). Besides, the Mn-Mn inter-chain distance is 10.333 Å. When considering these hydrogen bonds and π…π stacking interactions involving adjacent Trz ligands and chloride ions, we may consider the formation of a periodic pseudo 3-D polymeric network along the (*c, a*) plane as represented in **Figure 2**.

**2.2. Thermal analyses and FT-IR Spectroscopy**

The TGA-DSC profiles of the Mn(II) halide complex, as reported in **Figure 3**, indicate an initial mass loss detected between 380K and 481K approximately, corresponding to the release of the organic ligand. During this process, the sample lost 23% of its weight. This latter is accompanied by two successive endothermic peaks observed on the DSC curve at around 416K and 493K. Such phenomenon leads to the collapse of the polymeric network. This peak is then followed by two steps of weight loss accompanied by two endothermic DSC signals, corresponding to the sublimation of HCl. Beyond this temperature, a decomposition of $MnO_2$ oxide is observed in the 482-750 K range (42.5 %) and followed by an exothermic peak at 642K.

The vibrational study through room temperature infrared spectroscopy was undertaken in order to obtain more information about the structure feature.

The infrared spectrum of the title compound is shown in **Figure S4**. According to previous work on similar compounds [47-52], the FT-IR spectrum of the Mn(II) complex exh exhibits a broad absorption peak at 3138 $cm^{-1}$, which is assigned to the C-H vibration of the Trz ligand. The vibration peak at 2867 $cm^{-1}$ is attributed to the $NH_2$ stretching of the complex. In addition, the characteristic peak at 1640 $cm^{-1}$ is assigned to the $\delta NH_2$ bending. A series of intensity bonds ranging from 601 to 1529 $cm^{-1}$ are associated with the vibration modes of the aromatic skeleton.

## 2.3. Magnetic study

To gain further insight about the magnetic properties, the variable-temperature magnetic of the χT product under a magnetic field of 499.7 Oe is illustrated in **Figure 4a**. At 400K, the χT value is 0.01787 emu $mol^{-1}$ K $Oe^{-1}$ which is close to the spin-only value expected for two magnetically uncoupled Mn(II) cores with S = 5/2 and g=2.

Upon cooling from 400 to 2K, the χT product increases monotonically until reaching a maximum of 0.02 emu $mol^{-1}$ K $Oe^{-1}$ to 227 K, below which it begins to decrease. This behavior suggests the presence of magnetic order of spin-orbital coupling interactions mediated through bridging $\mu_2$-Cl and $\mu_2$-$N_1$, $N_2$-Trz ligands in the low temperature region.

**Figure 4.b** depicts the temperature dependence of the magnetic susceptibility and reciprocal susceptibility (χ(T) and $\chi^{-1}$(T)) of the crystalline compound. The former rises smoothly with decreasing temperature until it reaches a maximum of 0.047 emu $mol^{-1}$ $Oe^{-1}$ at 22K. Below this temperature, the susceptibility plot drops abruptly, reaching a value at 3K, then it increases until reaching a value of 0.041 emu $mol^{-1}$ $Oe^{-1}$ at 2K. In the paramagnetic region, the magnetic data follows the Curie-Weiss law described by the following relation $\chi = T/(T-\theta)$. A linear fit of $\chi^{-1}$ cures between 80 and 300 K gives a Curie constant of C=0.3534 (5) emu K $mol^{-1}$ and a Weiss constant of -45.8 K. In fact, the negative value of the Weiss temperature suggests the presence of antiferromagnetic interactions. The unexpected increase in Temperature below 3K clearly indicates a change in magnetic behavior, which could be due to canted antiferromagnetic exchange interactions (known as weak-ferromagnets) between neighboring Mn(II) carriers. This phenomenon is may be due to the distorted environment of the central atoms. Indeed, the magnetic interaction at high temperatures is dominated by antiferromagnetic coupling interactions, whereas the low-temperature magnetic behavior is attributed to a week ferromagnetic correlation attributed to the spin canting behavior. These different interactions are already observed for similar hybrid materials [53-55].

The theoretical value of the Curie constant $\mu_{eff}^{th}$( $\mu_\beta$) predicted for one Mn (II) center (s = 5/2, g = 2) is obtained by the following relation: $C = \frac{N g^2 \mu_B^2 S(S+1)}{3K}$, where k: Boltzmann's constant, N: the Avogadro's number, μB: the Bohr magnetron).

The value of the effective magnetic moment $\mu_{eff}$ of the complex deduced from the Curie constant according to the following expression $\mu_{eff}^{exp}$( $\mu_\beta$) = $(8C)^{1/2}$ is 4.47μB.

The field-dependence of the isothermal magnetization of the sample at 2 K which represents the hysteresis loops is depicted in **Figure 4.c**. The M(H) plot steadily rises until

reaching a saturation value of 7.5 μB per formula unit at 1kOe. In fact, this value is considerably lower than expected for two Mn (II) atoms with S = 5/2 and g=2 which supports the occurrence of antiferromagnetic ordering as well as the canted ferromagnetic coupling exchange interaction mediated through bridged Mn-Cl-Mn.

**2.4. Photo-physical investigation**

One of our concerns is to correlate the crystal structure with their physical properties, optical studies have been conducted therefore. **Figure 5** illustrates the room temperature solid-state photoluminescence spectra measured under a 266 nm excitation source for the complex as well as the Trz.Cl organic salt used as a reference. The deconvolution of the normalized Pl spectrum of the sample shows a bright bluish emission, Gaussian-shaped bond, around 464 nm (2.67 eV) accompanied by two weak shoulders at around 408 nm (3.04 eV) and 503 nm (2.46 eV). Furthermore, the Pl spectrum of the organic salt shows a single strong band in the UV region at around 374 nm (3.31 eV). By comparing the Pl spectrum of the complex with that of the corresponding Trz.Cl, we can conclude that bands around 408 and 374 nm are associated with the π-π* transition within the organic Trz ligands, while the two shoulder bands located around 464 and 503 nm are attributed, respectively, to the inorganic excitons confined within Mn(II) octahedral and to the d-d-type electronic transition produced by $((t^2g)^3 (eg)^2 \rightarrow (t^2g)^4 (eg)_1)$ transition [56-65].

It is to be noticed that the large blue-shift stocks (~34 eV) and the full width at half maximum (FWHM) observed in the emission spectrum of the organic salt compared to that of the complex are due to the significant distortion caused from the Jahn Teller effect within Mn(II) octahedral.

For the title compound, the broad-band emission yields to CIE color coordinates of (0.27, 0.35). The emitted color is visualized on the CIE 1931 chromaticity diagram (**Figure 6. a, b**). In addition, the correlated color temperature (CCT) is 8092 K which corresponds to a cold bluish light, and a high color rendering index (CRI) value of 96. Interestingly, the CRI value is equal to 96, which is among the highest values other compared to hybrid perovskite materials CRI values (**Table 1**) and surpassed even the high CRI indexes above 90 reported by several mixed-phosphor light sources. It is noteworthy to mention that most commercial WLEDs at present have a CRI values of approximately 80, which is considered adequate for daily lighting usage. However, Wight Light (WL) emission with a CRI > 90 is recommended in specific industries, including cosmetic sales counters, surgery, museum exhibitions, and also in cinematography [66,67].

According to **Table 1**, hybrid chloride materials reveals the highest CRI value which well agreed with the Dohner [68] et *al.* hypothesis that chloride substitution improves the light emission properties of the materials especially the CRI parameter. As a matter of fact, the broad bluish light emission as well as the high CRI value clearly reveals that the synthesis complex is a good candidate for a large area of lightning industrial application.

**Figure 7.a** illustrates the normalized absorption spectra (OA) of the complex and the organic salt measured at room temperature. The OA spectrum of the complex shows a broad intense band with a maximum intensity at 323 nm (3.8 eV) accompanied by two weaker bands around 432 nm (2.8 eV) and 485 nm (2.55 eV). For the OA spectrum of the Trz.Cl salt, a sharp signal edge was observed at 286 nm (4.33 eV). The comparison of these two spectra clearly shows that band located at 323 and 286 nm are associated with the π-π transition of the organic ligand. Besides, the band located at 432 nm is assigned to the inorganic excitons confined within the metal halide ions which are typically characteristic of the well-known Wannier-type excitons. Finally, the band located at 485 nm is due to the d-d electronic transition.

The PLE spectrum reveals the presence of a sharp excitonic band at 305 nm (4.06eV), in good agreement with the absorption measurements, associated with the π-π* transition.

These observations clearly reveal an occurrence of an energy transfer process where the organic and inorganic entities contribute to the emission process.

It is known that the RET process (or electronic energy transfer) is a radiative or non-radiative interaction mechanism describing the energy transfer that occurs from a luminophore donor molecule in its excited states with high band HOMO-LUMO Gap to an acceptor chromophore molecule with a smaller band HOMO-LUMO Ga[63-62]. The efficiency of this process depends on the distance between the donor and the acceptor molecules and the spectral overlap between the donor emission and the acceptor absorption spectra. It is to be mentioned that the RET mechanism can be accompanied by a charge transfer process when the donor and acceptor entities are separated by a distance of few angstroms. This phenomenon has been already observed in previously reported metal-halide perovskite materials comprising aromatic cations such us $(C_6H_{13}N_3)PbBr_4$ [60], $(C_3H_8N_6)PbCl_4$ [61], and $[C_6N_2H_5]_3BiCl_6$ [62]. In order to confirm these contribution, we superposed the PL spectrum of the complex and its OA spectrum (**Figure 7.b**). As reported in this figure, a significant overlap is observed between the emission band associated with the triazolate ligands (π-π* intra-ligand transition) and the absorption band of the Mn-Cl groups. In addition, the crystal

structure investigation shows that these entities are linked to each other through coordination interactions, indicating that the distance between them is approximately 2.23(2) Å, which fosters the RET as well as the charge transfer processes.

**Density of State modeling**

In order to better understand the contribution of the resonant energy transfer process, we carried out DFT simulation. The partial density of states (P-DOS) of inorganic moieties (Mn (II) and chlorine atoms) and organic moieties within the complex are plotted in **Figure 8a, b** respectively. A careful examination of the valence band (VB) of the sample shows that this latter is composed of C(2p) and N(2p) atomic orbitals mixed with a low contribution of Mn (3s) and Cl (3s) states. The conduction band (BC) comes from the 4p states of Mn and 3p states of Cl as well as a minor contribution from anti-binding interactions of C(2p) and N(2p). Note that the Mn(3s) and Cl(3s) states are located between -1.0 eV and the Fermi level (0 eV) while the HOMO levels of C(2p) and N (2p) states are located between -0.7 eV and 0 eV. We notice the appearance of sharp sub-bands composed of Mn (4p) and Cl1,2 (3p) states around 1.5 and 2.2 eV.

These latter are perfectly superposed in terms of energy with anti-binding C(2p) and N(2p) states within the Trz organic groups. Such theoretical investigations suggest a strong interaction between the inorganic and organic groups, thus confirming the occurrence of energy transfer and charge transfer processes between the two sub-lattice. In order to better describe the excitonic recombination process within this complex, we have examined the energy diagram leading to the strong bluish luminescent emission of the sample (**Figure 10)**. In this diagram, the RET process has been characterized in terms of the HOMO-LUMO transitions of the organic ligand on the first hand and the excitonic transition of the inorganic clusters on the other hand.

In a first step, the charge carriers localized within the organic ligands in their valence band are excited from the binding π to the anti-binding π* levels, creating Frenkel-type excitons. Simultaneously, electrons located within the inorganic valence band are excited to the 3p Manganese orbitals of the conduction band. These electrons form holes, leaving in the BV inorganic exciton quasi-localized within the Mn-Cl inorganic cluster. These latter are supposed to be of Mott-Wannier type exciton [60,61,65].

Furthermore, the energy of the organic Frenkel exciton is resonantly transferred, through a non-radiative process, to the inorganic groups. Thus, the population of charge carriers of the inorganic groups located in the BC increases, leading to the increase of the Mot-Wannier

exciton density. Then, the radiative process occurs and the recombination of the electron-hole pairs takes place within the inorganic levels. Thus, the RET process can be described as a conversion of Frenkel type exciton (Trz ligands) to the Mett-Wannier type exciton (inorganic Mn-Cl groups) (**Figure 9**).

## Conclusion

The main conclusion of the present work is to investigate a novel eco-friendly coordination polymer based on Mn(II) for interesting applications in the fields of optoelectronics. The single-crystal structure investigation showed that the structure packing consists of an unusual 1D helical crystal formed through edge-sharing Mn(II) octahedron linked through triazolate and chloride ligands. Furthermore, hydrogen bonds as well as π...π interactions between neighboring helical chains contribute to the pseudo-3-D polymeric network. A deep investigation of the magnetic properties revealed the coexistence of ferro and antiferromagnetic interactions between metal clusters. In fact, magnetic interaction at high temperature is dominated by antiferromagnetic coupling, while at low temperature, the deviation from the antiferromagnetic state showed weak ferromagnetic interactions. Besides, the photoluminescence study revealed the presence of strong bluish light emission with a very high CRI value of 96. The optical absorption study supported by DFT calculation revealed the presence of an RET process between organic and inorganic sub-lattices, leading to the conversion of Frenkel excitons localized within the organic part to Mott-Wannier excitons localized in inorganic clusters. Such behavior resulted in the intense emission of the complex.

We believe that the present work paves the way for the construction and design of novel coordination polymers that can potentially be a suitable alternative to hybrid perovskite materials to achieve environment-friendly solar cells, enrich the restricted WLED materials list and /or for the design of novel electromagnetic devices.

## Author Contributions

The manuscript was written by contributions of all authors. All authors have given approval to the final version of the manuscript.

## Notes

The authors declare no competing financial interest.


## ACKNOWLEDGMENT

A great thanks for ICMCB Bordeaux France, specially the XR diffraction service and Institute of NEEL, Grenoble France for magnetic measurements.

## ABBREVIATIONS

Trz: triazole

SEM : Scanning Electron Microscopy

## ASSOCIATED CONTENT

This material is available free of charge via the Internet at http://pubs.acs.org."

Supplementary crystallographic data for this article in CIF format are available as electronic supplementary publication from Cambridge Crystallographic Data Centre (CCDC: 2172103). This data can be obtained free of charge via https://www.ccdc.cam.ac.uk/community/deposita structure/CSD Communications/, or from the Cambridge Crystallographic Data Centre, 12 Union Road, Cambridge CB2 1EZ, UK (Fax: (international): +441223/336033; e-mail: deposit @ ccdc.cam.ac.uk).

# Highlights

- Crystal structure study reveals an unusual 1-D left-right handed helical crystal structure formed through edge-sharing Mn(II) octahedra.
- Magnetic properties reveal the occurrence of antiferromagnetic and spin canted interactions between metal clusters.
- Photoluminescence study reveals the presence of bright bluish light emission with very high CRI value.
- Optical study supported by DFT calculation confirms the presence of resonant energy transfer process between organic and inorganic sub-lattices.

# Figures

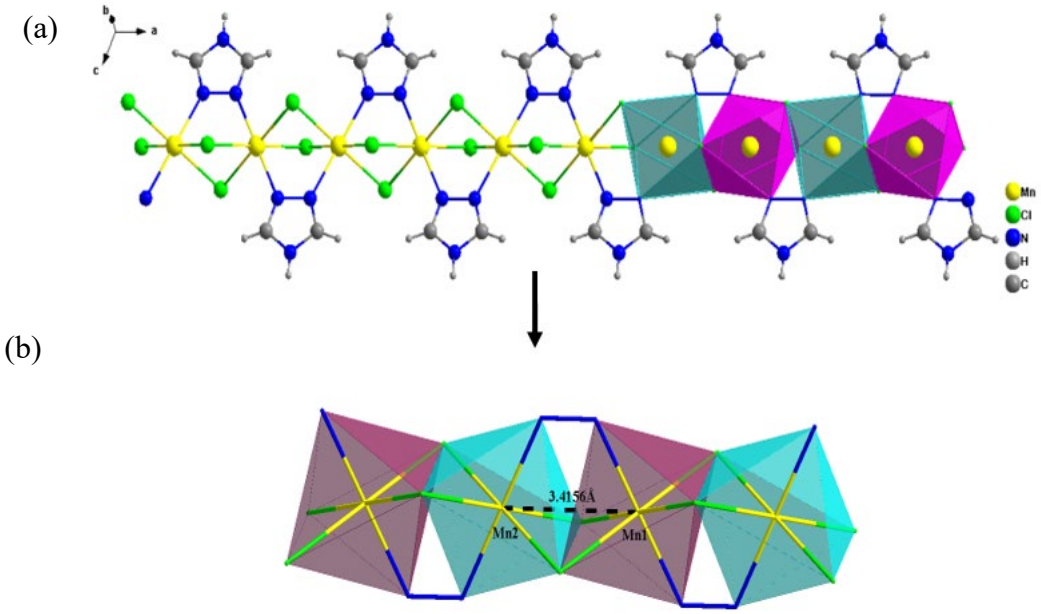


**Figure 1: a.** View of the one-dimensional substructure of Mn($\mu_2$-Trz)($\mu_2$-$Cl_2$), **b.** The coordination sphere of Mn(II) centers forming a distorted octahedral

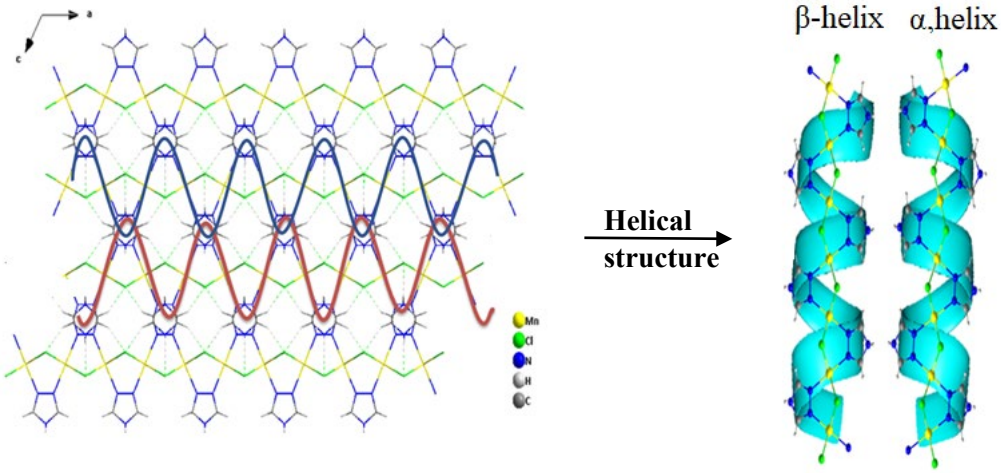


**Figure 2:** View of the polymeric network along the *b* axis showing the left-right handed helix chains

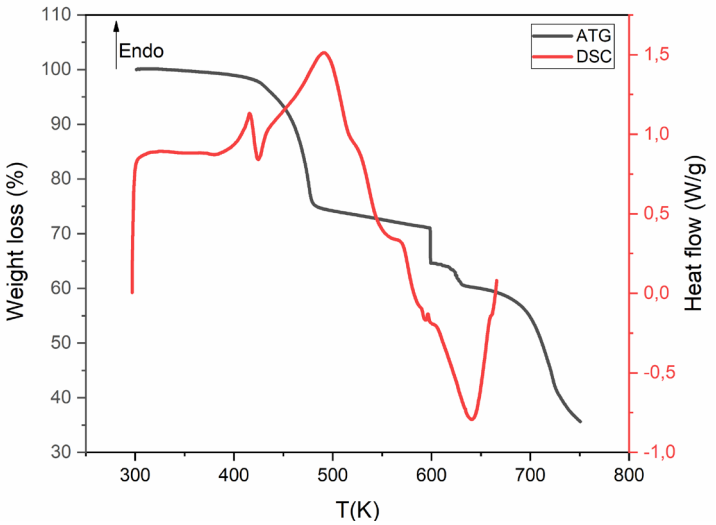


**Figure 3:** TGA-DSC curves for Mn($\mu_2$-Trz)($\mu_2$-$Cl_2$)

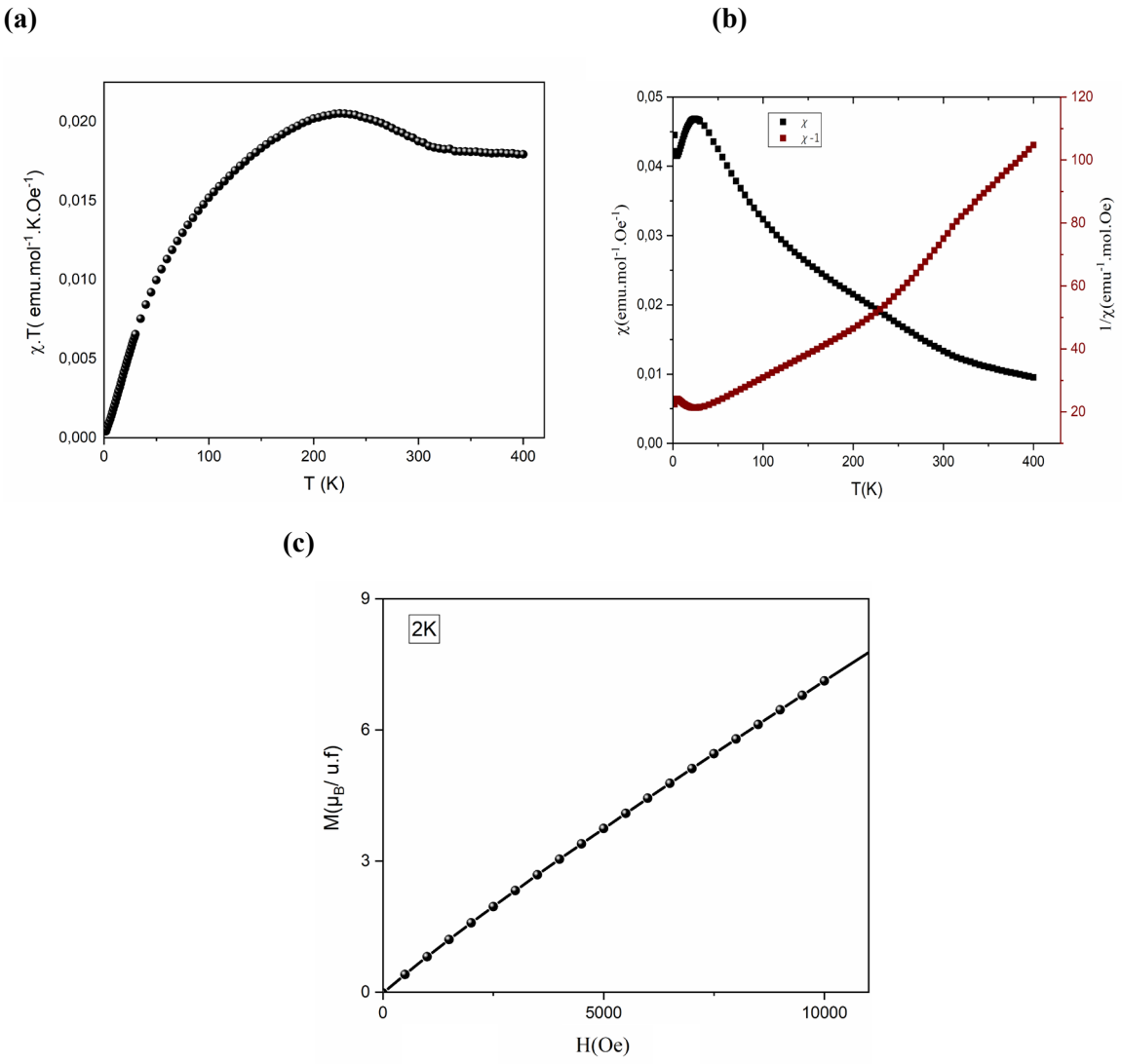


**Figure 4. a** Variation of χT data as a function of temperature, **b.** Temperature dependence of the susceptibility and reciprocal susceptibility for the Mn($\mu_2$-Trz)($\mu_2$-$Cl_2$) compound, **c.** The field-dependence of the isothermal magnetization at 2 K

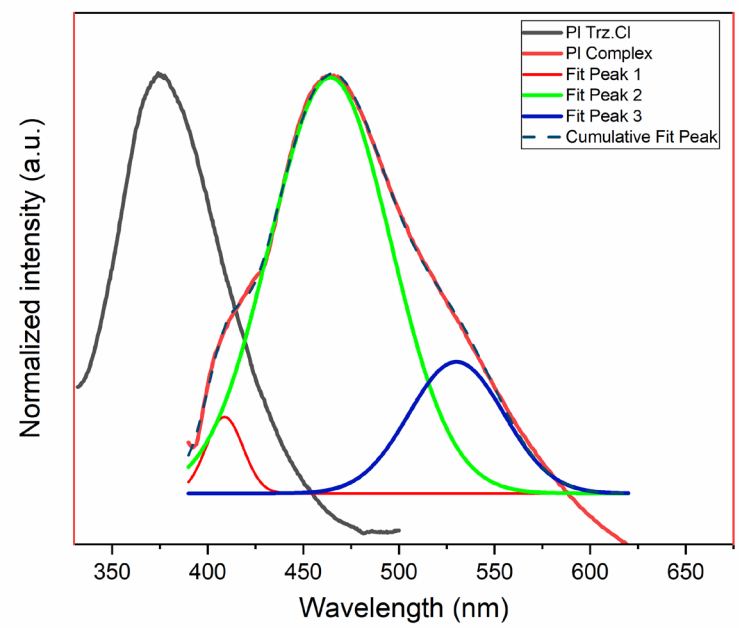


**Figure 5.** The room temperature solid-state photoluminescence spectra for the Mn(II)-based coordination polymer and the organic salt Trz.Cl

**(a)** **(b)**

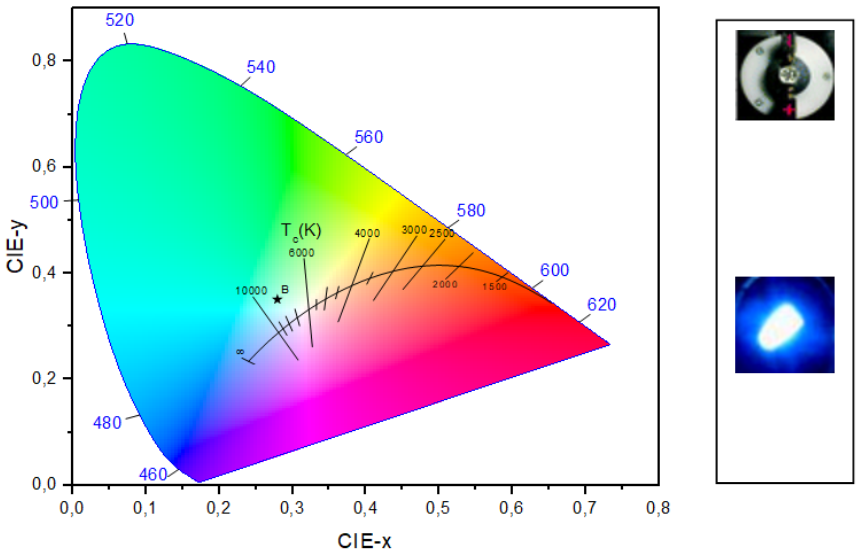


**Figure 6. a**. CIE chromaticity coordinates of the complex, **b.** Image of the Mn(II)-based complex crystals under before and during Pl analysis

**(a)** **(b)**

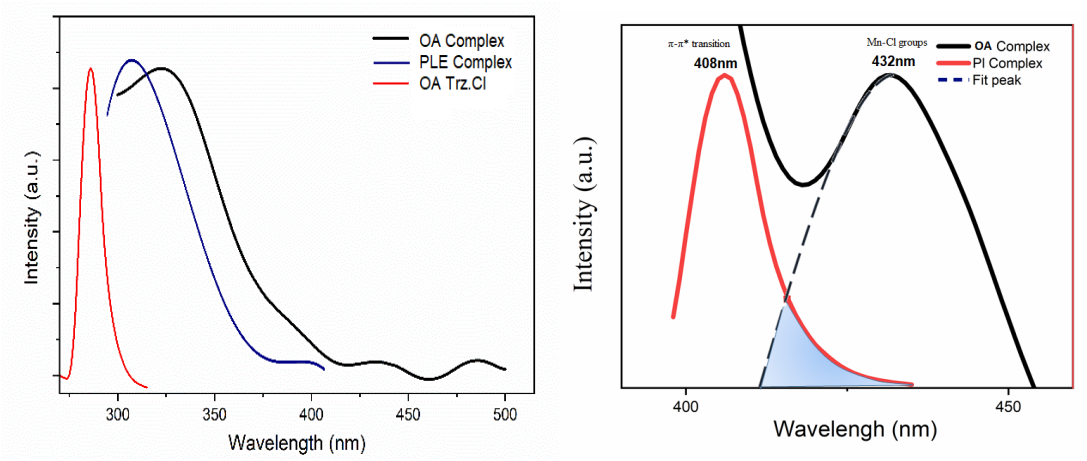


**Figure 7. a** OA spectrum of the complex, OA spectrum of the organic salt (Trz.Cl), and Room temperature photoluminescence excitation (PLE) of the complex recorded at room temperature, **b**. Spectral overlap between the emission spectrum of the organic ligand (donor) and the absorption spectrum of the inorganic clusters (acceptor)

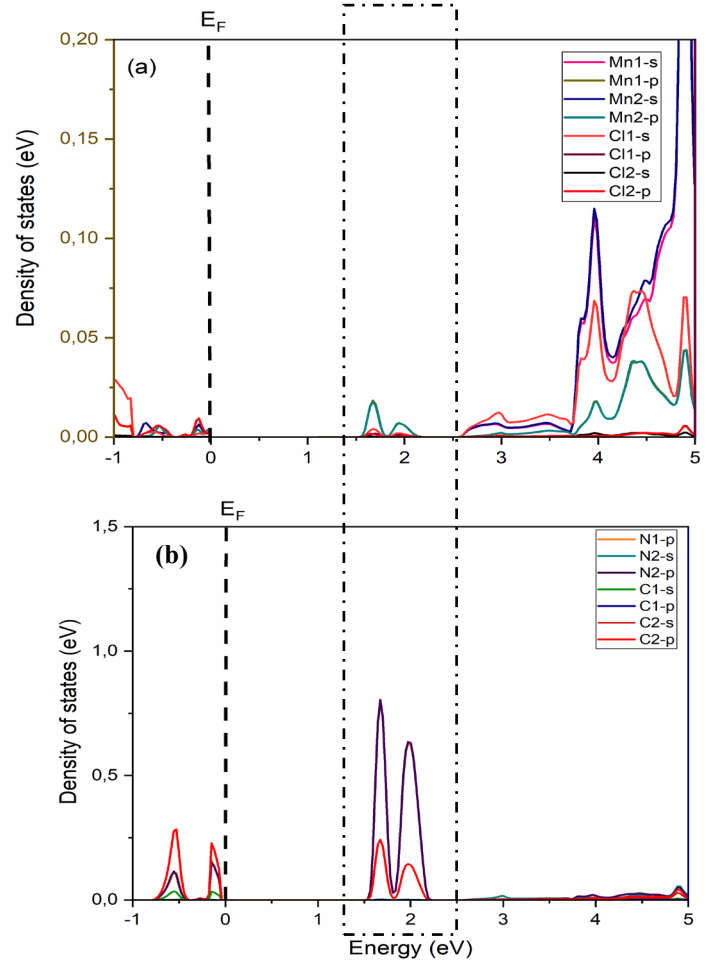


**Figure 8.** Calculated electronic density of states of the complex with **(a)** Density of states of manganese and chlorine atom orbitals within the complex, **(b)** Density of states of carbon and nitrogen atom orbitals within the complex

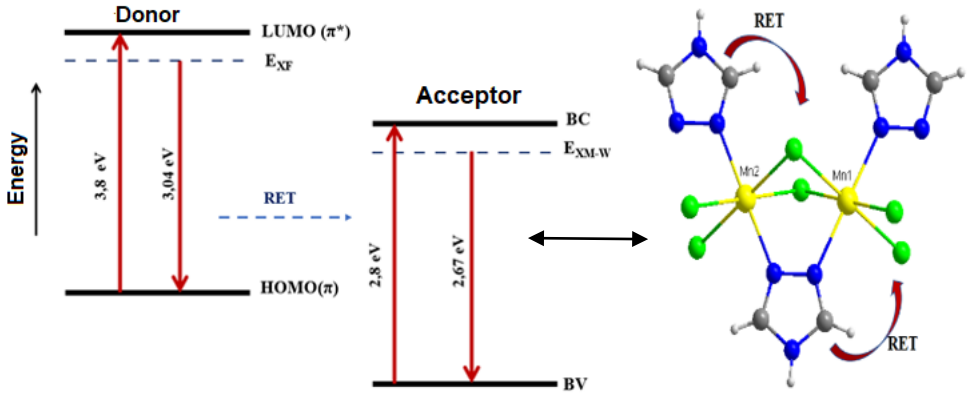


**Figure 9.** Energy diagram illustrating the RET mechanism of the Mn(μ-Trz) (μ-$Cl_2$) complex

# Table

**Table 1.** Light emission characteristics of previously reported halide based hybrid materials

| | Light emission characteristics | | | |
|---|---|---|---|---|
| **Hybrid Compound** | **Pl** | **CIE (x, y)** | **CCT (K)** | **CRI** |
| **(NMEDA ) $PbBr_4$** [68] | 2.22 | 0.36, 0.41 | 4669 | 82 |
| **$C_4N_2H_{14}$ $PbBr_4$** [69] | 2.61 | 0.21, 0.28 | 21392 | 63 |
| **$(C_4H_9NH_3)_2PbCl_4$** [70] | 2.28 | 0.37, 0.40 | 4423 | 86 |
| **$(C_5H_{14}N_2)PbCl_4 \cdot H_2O$** [71] | 2 | 0.39, 0.37 | 3445 | 94 |
| **$C_6H_{12}N_3PbCl_4$** [72] | 2.16 | 0.36, 0.37 | 4203 | 93 |
| **$(TAE)_2[Pb_2Cl_{10}](Cl)_2$** [22] | 2.51 | 0.30, 0.33 | 6741 | 96 |
| **$Mn_2(\mu_2\text{-}Trz)(\mu_2\text{-}Cl_2)$** | 2.67 | 0.27, 0.35 | 8092 | 96 |

## References

(1) Pode, R. Organic Light Emitting Diode Devices: An Energy Efficient Solid State Lighting for Applications. Renew. Sustain. Energy Rev. 2020, 133, 110043. https://doi.org/10.1016/j.rser.2020.110043.

(2) Rreza, I.; Yang, H.; Hamachi, L.; Campos, M.; Hull, T.; Treadway, J.; Kurtin, J.; Chan, E. M.; Owen, J. S. Performance of Spherical Quantum Well down Converters in Solid State Lighting. ACS Appl. Mater. Interfaces,2021,13(10),12191–12197. https://doi.org/10.1021/acsami.0c15161.

(3) Hao, F.; Stoumpos, C. C.; Cao, D. H.; Changand, R. P. H.; Kanatzidis, M. G. Lead-free solid-state organic-inorganic halide perovskite solar cells. Nat. Photonics 2014, 82, 1−6. https://doi.org/10.1038/nphoton.2014.82.

(4) Green, M. A.; Baillie, A. H.; Snaith, H. J. The emergence of perovskite solar cells. Nat. Photonics 2014, 8, 506−514.

(5) U.S. Department of Energy and Optoelectronics Industry Development Association. The Promise of Solid State Lighting for General Illumination ; Optoelectronics Industry Development Association: Washington DC, 2002.

(6) Wang, M. S.; Guo, S. P.; Li, Y.; Cai, L. Z.; Zou, J. P.; Xu, G.; Zhou, W. W.; Zheng, F. K.; Guo, G. C. Direct White-Light-Emitting Metal-Organic Framework with Tunable Yellow-to-White Photoluminescence by Variation, J Am Chem Soc 2009,131(38),13572-3. https://doi.org/10.1021/ja903947b.

(7) Sehrawat, P.; Khatkar, A.; Boora, P.; Hooda, A.; Kumar, M.; Malik, R. K.; Khatkar, S. P.; Taxak, V. B. A Novel Strategy for High Color Purity Virescent Er3+-Doped SrLaAlO4 Nanocrystals for Solid-State Lighting Applications. J. Mater. Sci. Mater. Electron. 2020, 31 (8), 6072–6083. https://doi.org/10.1007/s10854-020-03160-w.

(8) Singh, R. K., Sharma, P., Lu, C. H., Kumar, R., Jain, N., & Singh, J. (2021). Structural, morphological and thermodynamic parameters investigation of tunable MAPb1−xCdxBr3–2xI2x hybrid perovskite. *Journal of Alloys and Compounds*, *866*. https://doi.org/10.1016/j.jallcom.2021.158936

(9) Benabdallah, I., Boujnah, M., El Kenz, A., Benyoussef, A., Abatal, M., & Bassam, A. (2019). Lead-free perovskite based bismuth for solar cells absorbers. *Journal of Alloys and Compounds*, *773*, 796–801. https://doi.org/10.1016/j.jallcom.2018.09.332

(10) Li, X.; Fu, Y.; Pedesseau, L.; Guo, P.; Cuthriell, S.; Hadar, I.; Even, J.; Katan, C.; Stoumpos, C. C.; Schaller, R. D.; Harel, E.; Kanatzidis, M. G. Negative Pressure Engineering with Large Cage Cations in 2D Halide Perovskites Causes Lattice Softening. J. Am. Chem. Soc. 2020, 142 (26), 11486–11496. https://doi.org/10.1021/jacs.0c03860.

(11) Lee, A. Y., Park, D. Y., & Jeong, M. S. (2018). Correlational study of halogen tuning effect in hybrid perovskite single crystals with Raman scattering, X-ray diffraction, and absorption spectroscopy. *Journal of Alloys and Compounds*, *738*, 239–245. https://doi.org/10.1016/j.jallcom.2017.12.149

(12) Yang, W. S.; Park, B. W.; Jung, E. H.; Jeon, N. J.; Kim, Y. C.; Lee, D. U.; Shin, S. S.; Seo, J.; Kim, E. K.; Noh, J. H.; Seok, S. I. Iodide management informamidinium-lead-halide-based perovskite layers for efficient solar cells. Science 2017, 356 (6345), 1376−1379.https://10.1126/science.aan2301.

(13) Ortega, E.; Aranguren, G.; Jimeno, J. C. Photovoltaic Modules Transient Response Analysis and Correction under a Fast Characterization System. Sol. Energy 2021, 221,232–242. https://doi.org/10.1016/j.solener.2021.03.032.

(14) Mei, Y., Shen, Z., Kundu, S., Dennis, E., Pang, S., Tan, F., ... & Saidaminov, M. I. Perovskite Solar Cells with Polyaniline Hole Transport Layers Surpassing a 20% Power Conversion Efficiency. Chem. Mater. 2021, 33, 4679–4687. https://doi.org/10.1021/acs.chemmater.1c01176.

(15) Yao, T., Bo, X., Peng. X, Yubo. L., Qinghui. J., and J. Y. M. , Photovoltaic Performance of Flexible Solar Cells with Semitransparent Inorganic Perovskite Active Layers by Interface Engineering. Am. Chem. Soc. 2021, 13, 20034–20042. https://doi.org/10.1021/acsami.1c01674.

(16) Xu, Y.; Yao, H.; Ma, L.; Wu, Z.; Cui, Y.; Hong, L.; Zu, Y.; Wang, J.; Woo, H. Y.; Hou, J. Organic Photovoltaic Cells with High Efficiencies for Both Indoor and Outdoor Applications. Mater. Chem. Front. 2021, 52, 893–900. https://doi.org/10.1039/d0qm00633e.

(17) Mainville, M.; Leclerc, M. Recent Progress on Indoor Organic Photovoltaics: From Molecular Design to Production Scale. ACS Energy Lett. 2020, 5 (4), 1186–1197. https://doi.org/10.1021/acsenergylett.0c00177.

(18) Mao, L.; Wu, Y.; Stoumpos, C. C.; Wasielewski, M. R.;
Kanatzidis, M. G. White-Light Emission and Structural Distortion in New Corrugated Two-Dimensional. J. Am. Chem. Soc. 2017, 139, 14, 5210–5215. https://doi.org/10.1021/jacs.7b01312.

(19) Safie, N. E.; Azam, M. A.; Aziz, M. F. A.; Ismail, M. Recent Progress of Graphene-Based Materials for Efficient Charge Transfer and Device Performance Stability in Perovskite Solar Cells. Int. J. Energy Res. 2021, 45 (2), 1347–1374. https://doi.org/10.1002/er.5876.

(20) Hatae, T.; Koshiyama, T.; Ohba, M. Domain Size Dependent Fluorescence Resonance Energy Transfer in Lipid Domain Incorporated Fluorophores. Chem. Lett. 2017, 46 (5), 756–759. https://doi.org/10.1246/cl.170104.

(21) Dammak, T.; Abid, Y. Quasi-white light emission involving Forster resonance energy transfer in a new organic inorganic tin chloride based material (AMPS)[$SnCl_6$]$H_2O$. Opt. Mater. 2017, 66, 302−307. https://10.1016/j.optmat.2017.02.020

(22) Elleuch, S.; Lusson, A.; Pillet, S.; Boukheddaden, K.; Abid, Y. White Light Emission from a Zero-Dimensional Lead Chloride Hybrid Material. ACS Photonics 2020, 7 (5), 1178–1187. https://doi.org/10.1021/acsphotonics.9b01817.

(23) Mitzi, D. B.; Chondroudis, K.; Kagan, C. R. Organic-inorganic electronics. IBM J. Res. Dev. 2001, 45 (1), 29−45.

(24) J. Cao and F. Yan, Energy Environ. Sci., 2021, 14, 1286–1325.

(25) Dutta, B.; Das, D.; Datta, J.; Chandra, A.; Jana, S.; Sinha, C.; Ray, P. P.; Mir, M. H. Synthesis of a Zn(Ii)-Based 1D Zigzag Coordination Polymer for the Fabrication of Optoelectronic Devices with Remarkably High Photosensitivity. Inorg. Chem. Front. 2019, 6 (5), 1245–1252. https://doi.org/10.1039/c9qi00162j.

(26) Li, Y.; Lu, S. H.; Zhao, R. D.; Lu, Z. X.; Liu, X. L.; Qin, Y.; Yang, S. X.; Zheng, L. Y.; Cao, Q. E. A Stable 1D Helical Silver Coordination Polymer with Red Emission. Polym. Chem. 2019, 10 (21), 2653–2657. https://doi.org/10.1039/c9py00362b.

(27) Xu, W.; Jiang, F.; Zhou, Y.; Xiong, K.; Chen, L.; Yang, M.; Feng, R.; Hong, M. Three Novel Organic-Inorganic Complexes Based on Decavanadate [V 10O 28] 6- Units: Special Water Layers, Open 3D Frameworks and Yellow/Blue Luminescences. Dalt. Trans. 2012, 41 (25), 7737–7745. https://doi.org/10.1039/c2dt30532a.

(28) Yu, W., Jia, X., Long, Y., Shen, L., Liu, Y., Guo, W., & Ruan, S. Highly efficient semitransparent polymer solar cells with color rendering index approaching 100 using one-dimensional photonic crystal. ACS Applied Materials & Interfaces, 2015, 7(18), 9920-9928. https://doi.org/10.1021/acsami.5b02039.

(29) Tang, Y.; Wu, H.; Cao, W.; Cui, Y.; Qian, G. Luminescent Metal–Organic Frameworks for White LEDs. Adv. Opt. Mater. 2021, 9 (23), 1–14. https://doi.org/10.1002/adom.202001817.

(30) García-García, A.; Zabala-Lekuona, A.; Goñi-Cárdenas, A.; Cepeda, J.; Seco, J. M.; Salinas-Castillo, A.; Choquesillo-Lazarte, D.; Rodríguez-Diéguez, A. Magnetic and Luminescent Properties of Isostructural 2d Coordination Polymers Based on 2-Pyrimidinecarboxylate and Lanthanide Ions. Crystals 2020, 10 (7), 1–12. https://doi.org/10.3390/cryst10070571.

(31) Yu, M. X. ; Liu, C. P. ; Zhao, Y. F. ; Li, S. C. ; Yu, Y. L. ; Lv, J. Q. ; Lian, C. ;Fei, M J.;Hong, M. C.. White-Light Emission and Circularly Polarized Luminescence from a Chiral Copper (I) Coordination Polymer through Symmetry-Breaking Crystallization. Angewandte Chemie International Edition, 2022, e202201590. https://doi.org/10.1002/anie.202201590.

(32) Hatae, T.; Koshiyama, T.; Ohba, M. Domain Size Dependent Fluorescence Resonance Energy Transfer in Lipid Domain Incorporated Fluorophores. Chem. Lett. 2017, 46 (5), 756–759. https://doi.org/10.1246/cl.170104.

(33) Zhang, X.; Wang, W.; Hu, Z.; Wang, G.; Uvdal, K. Coordination Polymers for Energy Transfer: Preparations, Properties, Sensing Applications, and Perspectives. Coord. Chem. Rev. 2015, 284, 206–235. https://doi.org/10.1016/j.ccr.2014.10.006.

(34) Ouellette, W.; Prosvirin, A. V; Chieffo, V.; Dunbar, K. R.; Hudson, B.; Zubieta, J. Solid-State Coordination Chemistry of the Cu / Triazolate / X System. Inorg. Chem. 2006, 45 (23), 9346–9366.

(35) Roubeau, O.; Castro, M.; Burriel, R.; Haasnoot, J. G.; Reedijk, J. Calorimetric Investigation of Triazole-Bridged Fe(II) Spin-Crossover One-Dimensional Materials: Measuring the Cooperativity. J. Phys. Chem. B 2011, 115 (12), 3003–3012. https://doi.org/10.1021/jp109489g.

(36) Serhan, M.; Sprowls, M.; Jackemeyer, D.; Long, M.; Perez, I. D.; Maret, W.; Tao, N.; Forzani, E. Total Iron Measurement in Human Serum with a Smartphone. AIChE Annu. Meet. Conf. Proc. 2019, 2019-Novem. https://doi.org/10.1039/x0xx00000x.

(37) Wang, H.; Sinito, C.; Kaiba, A.; Costa, J. S.; Dagault, P.; Guionneau, P.; Létard, J.; Negrier, P.; Mondieig, D.; Wang, H.; Sinito, C.; Kaiba, A.; Costa, J. S.; Desplanches, C. Unusual Solvent Dependence of a Molecule-Based FeII Macrocyclic Spin-Crossover Complex 2014, 29, 4927-4933. https://doi.org/10.1002/ejic.201402666.

(38) Grosjean, A.; Négrier, P.; Bordet, P.; Etrillard, C.; Péchev, S.; Lebraud, E.; Létard, J.; Grosjean, A.; Négrier, P.; Bordet, P.; Etrillard, C.; Mondieig, D. Crystal Structures and Spin

Crossover in the Polymeric Material [ Fe ( Htrz ) 2 ( Trz )]( BF4 ) Including Coherent-Domain Size Reduction Effects 2018, 2, 1961-1966.
(39)Lakhloufi, S.; Lemée-Cailleau, M. H.; Chastanet, G.; Rosa, P.; Daro, N.; Guionneau, P. Structural Movies of the Gradual Spin-Crossover in a Molecular Complex at Various Physical Scales. Phys. Chem. Chem. Phys. 2016, 18 (40), 28307–28315. https://doi.org/10.1039/c6cp04987g.
(40) Ouellette, W.; Prosvirin, A. V; Chieffo, V.; Dunbar, K. R.; Hudson, B.; Zubieta, Coordination Chemistry of the Cu / Triazolate / X System. Inorg. Chem. 2006, 45 (23), 9346–9366.
(41) Richard, R; Marcel H; Maryana, K,Andreas, K; Anton, J; Dirk, V, Synthesis, Thermal Stability and Magnetic Properties of an Interpenetrated Mn(II) Triazolate Coordination Framework. Zeitschrift für anorganische und allgemeine Chemie, 2022, p. e202200153. https://doi.org/10.1002/zaac.202200153.
(42) Sheldrick, G; M. SHELXL-97, Progr. X-ray Cryst. Struct. Refinement; Gottingen Univ. Gottingen, Ger. 1997.
(43) L, J; F. J; Appl, Crystallogr 1999, 32, 837.
(44)Sheldrick, G. M; SHELXL-2018/1, Program for Crystal Structure Refinement University of Göttingen: Germany,. 2018.
(45) Dolomanov. O, L. Bourhis, Gildea, Howard. R, Olex2 Program. J. Appl. Cryst 2009, 42, 339.
(46) K, B. Diamond Version 4, 0, Impact GbR, Bonn, Germany. 2009.
(47) Ouellette, W.; Prosvirin, A. V.; Valeich, J.; Dunbar, K. R.; Zubieta, J. Hydrothermal Synthesis, Structural Chemistry, and Magnetic Properties of Materials of the MII/Triazolate/Anion Family, Where MII = Mn, Fe, and Ni. Inorg. Chem. 2007, 46 (22), 9067–9082. https://doi.org/10.1021/ic700790h.
(48) Depmeier, W. The Modulated Structure of the Layered Perovskite γ-Bis(n-Propylammonium) Tetrachloromanganate(II): Refinement of the Average Structure, the Possible Superspace Group and a Model for the Modulated Structure; Erratum. Acta Crystallogr. Sect. B Struct. Crystallogr. Cryst. Chem. 1981, 37 (6), 1322–1322. https://doi.org/10.1107/s0567740881005839.
(49)Miyasaka, H.; Okawa, H.; Miyazaki, A.; Enoki, T. Synthesis, Crystal and Network Structures, and Magnetic Properties of a Hybrid Layered Compound: [K(18-Cr)(2-PrOH)2][{Mn(Acacen)}2{Fe(CN)6}] (18-Cr = 18-Crown-6-Ether, Acacen = N,N′-

Ethylenebis(Acetylacetonylideneiminate)). Inorg. Chem. 1998, 37 (19), 4878–4883. https://doi.org/10.1021/ic980448p.

(50)Kanungo, S.; Saha-Dasgupta, T. First-Principles Study of Organic-Inorganic Hybrid Framework Compound Mn(C4H4O4). Phys. Rev. B - Condens. Matter Mater. Phys. 2011, 84 (13), 1–7. https://doi.org/10.1103/PhysRevB.84.134415.

(51)Grosjean, A.; Négrier, P.; Bordet, P.; Etrillard, C.; Mondieig, D.; Pechev, S.; Lebraud, E.; Létard, J. F. . G. , . Eur. J. Inorg. Chem. 2013, 796–802.

(52)Narsimhulu, P., Franck, T., Smail, T, Kamel, B., Guillaume, C., Cooperative 1D triazole-based spin crossover FeII material with exceptional mechanical resilience, M. M. Chem. Mater 2017, 29, 2, 490–494.

(53) Cao, C.; Liu, S. J.; Yao, S. L.; Zheng, T. F.; Chen, Y. Q.; Chen, J. L.; Wen, H. R. Spin-Canted Antiferromagnetic Ordering in Transition Metal-Organic Frameworks Based on Tetranuclear Clusters with Mixed V- and Y-Shaped Ligands. Cryst. Growth Des. 2017, 17 (9), 4757–4765. https://doi.org/10.1021/acs.cgd.7b00682.

(54)Mínguez. E; Coronado, E. Magnetic Functionalities in MOFs: From the Framework to the Pore. Chem. Soc. Rev. 2018, 47 (2), 533–557. https://doi.org/10.1039/c7cs00653e.

(55) Zhang, X. M.; Li, P.; Gao, W.; Liu, J. P. Spin-Canting Magnetization in 3D Metal Organic Frameworks Based on Strip-Shaped Δ-Chains. RSC Adv. 2015, 5 (94), 76752–76758. https://doi.org/10.1039/c5ra15937g.

(56) Kassou, S.; Belaaraj, A.; Guionneau, P.; Shaltaf, R. Crystal Structure, Optical and Electronic Properties Studies on an Hybrid Multifunctional MnCl4-Based Material. Adv. Compos. Hybrid Mater. 2019, 2 (2), 373–380. https://doi.org/10.1007/s42114-019-00093-9.

(57) Deng, Y.; Dong, X.; Yang, M.; Zeng, H.; Zou, G.; Lin, Z. Two Low-Dimensional Metal Halides: Ionothermal Synthesis, Photoluminescence, and Nonlinear Optical Properties. Dalt. Trans. 2019, 48 (47), 17451–17455. https://doi.org/10.1039/c9dt04102h.

(58) Andrews, D. L.; Bradshaw, D. S.; Dinshaw, R.; Scholes, G. D. Resonance Energy Transfer. Photonics Sci. Found. Technol. Appl. 2015, 4, 101–127. https://doi.org/10.1002/9781119011804.ch3.

(59) Pan, X.; Chen, H.; Wang, W. Z.; Ng, S. C.; Chan-Park, M. B. Resonance Energy Transfer (RET)-Induced Intermolecular Pairing Force: A Tunable Weak Interaction and Its Application in SWNT Separation. J. Phys. Chem. A 2011, 115 (28), 8155–8166. https://doi.org/10.1021/jp202978z.

(60) Barkaoui, H.; Abid, H.; Yangui, A.; Triki, S.; Boukheddaden, K.; Abid, Y. Yellowish White-Light Emission Involving Resonant Energy Transfer in a New One-Dimensional

Hybrid Material: (C9H10N2)PbCl4. J. Phys. Chem. C 2018, 122 (42), 24253–24261. https://doi.org/10.1021/acs.jpcc.8b06850.
(61) Medhioub, O.; Samet, A.; Barkaoui, H.; Triki, S.; Abid, Y. Multiexcitonic Broad-Band Emission Enhanced by Resonant Energy Transfer in a New Two-Dimensional Organic-Inorganic Perovskite: (C3H8N6)PbCl4. J. Phys. Chem. C 2020, 124 (37), 20359–20366. https://doi.org/10.1021/acs.jpcc.0c04768.
(62) Trabelsie, S.; Samet, A.; Dammak, H.; Michaud, F.; Santos, L.; Abid, Y.; Chaabouni, S. Optical Properties of a New Luminescent Hybrid Material [C6N2H5]3BiCl6 Involving a Resonance Energy Transfer (RET). Opt. Mater. (Amst). 2019, 89(1), 355–360. https://doi.org/10.1016/j.optmat.2019.01.015.
(63) Blumstengel, S.; Sadofev, S.; Xu, C.; Puls, J.; Henneberger, F. Converting Wannier into Frenkel Excitons in an Inorganic/Organic Hybrid Semiconductor Nanostructure. Phys. Rev. Lett. 2006, 97 (23), 8–11. https://doi.org/10.1103/PhysRevLett.97.237401.
(64) Yangui, A.; Roccanova, R.; McWhorter, T. M.; Wu, Y.; Du, M. H.; Saparov, B. Hybrid Organic-Inorganic Halides (C5H7N2)2MBr4 (M = Hg, Zn) with High Color Rendering Index and High-Efficiency White-Light Emission. Chem. Mater. 2019, 31, 2983−2991.
(65) Robinson, K.; Gibbs, G. V.; Ribbe, P. H. Quadratic Elongation: A Quantitative Measure of Distortion in Coordination Polyhedra. Science 1971, 172 (3983), 567−570.
(66) Liu, Z. F.; Wu, M. F.; Wang, S. H.; Zheng, F. K.; Wang, G. E.; Chen, J.; Xiao, Y.; Wu, A. Q.; Guo, G. C.; Huang, J. S. Eu3+-doped Tb3+ metal-organic frameworks emitting tunable three primary colors towards white light. J. Mater. Chem. C 2013, 1, 4634−3639.
(67) Wei, Y.; Li, Q.; Sa, R.; Wu, K. A white-light-emitting LnMOF with color properties improved via Eu3+ doping: analternative approach to a rational designfor solid-state lighting. Chem. Commun.
2014, 50, 1820−1823.
(68) Dohner, E. R.; Hoke, E. T.; Karunadasa, H. I. Self-Assembly of Broadband White-Light Emitters. J. Am. Chem. Soc. 2014, 136, 1718−1721.
(69)Yangui, A.; Roccanova, R.; Wu, Y.; Du, M. H.; Saparov, B. Highly Efficient Broad-Band Luminescence Involving Organic and Inorganic Molecules in a Zero-Dimensional Hybrid Lead Chloride. J. Phys. Chem. C 2019, 123, 22470−22477.
(70) Ji, C.; Wang, S.; Li, L.; Sun, Z.; Hong, M.; Luo, J. The First 2D Hybrid Perovskite Ferroelectric Showing Broadband White-Light Emission with High Color Rendering Index. Adv. Funct. Mater. 2019, 29, 1805038.

(71) Wang, S.; Yao, Y.; Wu, Z.; Peng, Y.; Li, L.; Luo, J. Realization of “warm” white light via halide substitution in polartwo-dimensional hybrid perovskites (2meptH2)PbClxBr4-x. J. Mater. Chem. C 2018, 6 (45), 12267−12272.
(72) Wu, Z.; Ji, C.; Sun, Z.; Wang, S.; Zhao, S.; Zhang, W.; Li, L.; Luo, J. Broadband white-light emission with a highcolor rendering index in a two-dimensional organic-inorganic hybrid perovskite. J. Mater. Chem. C 2018, 6, 1171−1175.